Computational Study of Key Mechanistic Details for a Proposed Copper(I)-Mediated Deconstructive Fluorination of *N*-Protected Cyclic Amines

Alexey L. Kaledin,[#] Jose B. Roque[||], Richmond Sarpong[||], and Djamaladdin G. Musaev*[,#]

[#] *Cherry L. Emerson Center for Scientific Computation, and Department of Chemistry, Emory University, Atlanta, GA 30322, USA.*

[||] *Department of Chemistry, University of California, Berkeley, CA 94720, USA.*

Corresponding Author: **dmusaev@emory.edu**

ABSTRACT: Using calculations, we show that a proposed Cu(I)-mediated deconstructive fluorination of *N*-benzoylated cyclic amines with Selectfluor® is feasible and may proceed through: (a) substrate coordination to a Cu(I) salt, (b) iminium ion formation followed by conversion to a hemiaminal, and (c) fluorination involving C–C cleavage of the hemiaminal. The iminium ion formation is calculated to proceed via a F-atom coupled electron transfer (FCET) mechanism to form, formally, a product arising from oxidative addition coupled with electron transfer (*OA+ET*). The subsequent *β*-C–C cleavage/fluorination of the hemiaminal intermediate may proceed via either ring-opening or deformylative fluorination pathways. The latter pathway is initiated by opening of the hemiaminal to give an aldehyde, followed by formyl H-atom abstraction by a $TEDA^{2+}$ radical dication, decarbonylation, and fluorination of the C3-radical center by another equivalent of Selectfluor®. In general, the mechanism for the proposed Cu(I)- mediated deconstructive C–H fluorination of *N*-benzoylated cyclic amines (**LH**) by Selectfluor® was calculated to proceed analogously to our previously reported Ag(I)-mediated reaction. In comparison to the Ag(I)-mediated process, in the Cu (I)-mediated reaction the iminium ion formation and hemiaminal fluorination have lower associated energy barriers, whereas the product release and catalyst re-generation steps have higher barriers.

Keywords: Deconstructive fluorination, *N*-benzoylated cyclic amines, Copper catalyst, Selectfluor®, DFT calculation, two-state Reactivity

1. INTRODUCTION

Computational studies have proven to be highly effective in guiding the development of novel synthetic methodologies including selective C–H and C–C bond functionalization [1-47]. Despite ongoing advances, the development of methods for selective C–H [48-64] and C–C [65-70] bond fluorination still remains a challenge. In this context, a promising strategy is the use of transition metal complexes and N−F reagents such as N-fluorobenzenesulfonimide (NFSI), N-fluoropyridinium salts (NFPy), and 1-chloromethyl-4-fluoro-1,4-diazoniabicyclo[2.2.2]octane bis(tetrafluoroborate) (Selectfluor®) [71-100]. These versatile N−F reagents have been shown to engage in electrophilic or radical fluorination reactions [80], in some cases participating in the cleavage of C−H bonds through processes described as single-electron transfer (SET) events [81.82]. When used in combination with transition metals, the metal complexes may also play multiple roles as either a promoter or catalyst [80,86,95]. For example, Lectka and coworkers [80] have shown that earth-abundant Cu(I) salts in combination with N–F reagents mediate C–H bond fluorination of aliphatic substrates. In this case, the Cu(I)-center mediates F-atom transfer from Selectfluor resulting in generation of a dicationic aminyl radical which abstracts a hydrogen atom from aliphatic substrates. In contrast, it is only recently that methods for fluorination that rely on C–C cleavage (e.g., decarboxylation) have begun to emerge. Selective C–C functionalization to access alkyl fluorides is an unusual transformation with opportunities to unearth new knowledge of practical benefit.

For fluorination reactions that rely on C–C cleavage, targeting C(sp^3)–C(sp^3) bonds in saturated heterocycles could open new horizons for the diversification of bioactive heterocycles given the prevalence of these structural motifs in pharmaceuticals and agrochemicals. Sarpong and coworkers [65,83-85] have recently reported a ring-opening fluorination method involving C–C cleavage that transforms *N*-protected saturated aza-cycles (e.g., **1** or **LH**, Scheme 1) into fluorine-containing acyclic amine derivatives (**LOF** and **LF**) using Selectfluor® (**2**; labeled as (F–TEDA)$^{2+}$), and $AgBF_4$ (i.e., Ag(I), below).

Scheme 1. Silver-Mediated Deconstructive Fluorination of *N*-Protected Cyclic Amine **1** (or **LH**) (see Ref. 83-85).

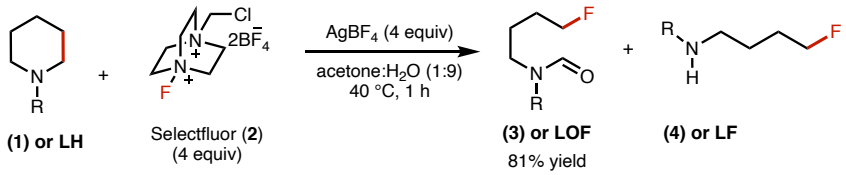

In a recent computational study by us [86], using existing experimental information [83-100], we showed that the first stage of the overall transformation, i.e., iminium ion formation (see Scheme 2a), begins with rapid generation of a singlet state adduct [(**LH**)-Ag], **5-s**, that binds [F-TEDA]$^{2+}$ to form singlet state intermediate [(**LH**)-Ag][F-TEDA]$^{2+}$, **6-s**. A subsequent addition of N–F across the Ag-center was characterized through calculations as a *F-atom coupled electron transfer (FCET)* event that proceeds through *two-state reactivity (TSR)* [101-108] triggered by singlet-to-triplet (S–T) seams of crossing [109]. The product of this event is [(**LH**$^+$)·-AgF·]–[TEDA]$^+$, **7-t**, which is a triplet state intermediate that could also arise from a formal *oxidative addition of the N–F group coupled with an electron transfer* (*OA+ET*) [110]. Rapid H-atom and F-atom coupling in intermediate **7-t** transforms it to the singlet state iminium-ion complex, [**L**$^+$-Ag]–HF–(TEDA)$^+$], **8-s**. Iminium-ion **8-s** traps H_2O to form singlet state hemiaminal **9-s**.

The subsequent C–C bond cleavage /fluorination of hemiaminal **9-s** occurs through either ring-opening (Path A) or deformylation (Path B). Path-A involves H-atom abstraction from hemiaminal **9-s** by the F-atom [of [F-TEDA]$^{2+}$] to form Ag-alkoxide intermediate **12-t**. This HAT/FAT process, which has a low energy barrier, is also a *TSR* event (see Scheme 2) and leads to the singlet state intermediate **13-s**. The C(sp^3)–F bond formation that completes Path A occurs through a formal fluorine atom transfer mechanism (shown in Scheme 2). The competing deformylative fluorination pathway (Path B) is initiated by equilibration of hemiaminal **9-s** to aldehyde **17-s**, followed by H-atom abstraction from the formyl group by a previously generated TEDA^{2+} radical dication, decarbonylation of the resultant **18-d** to form **19-d**, and fluorination of **19-d** by another equivalent of [F-TEDA]$^{2+}$. A decarboxylative fluorination mechanism involving heterolytic C–N bond cleavage and oxidation of the aldehyde to the carboxylic acid may also be operative.

We have shown that the electronic properties of the group on nitrogen is critical for both the iminium ion formation and C3-fluorination.

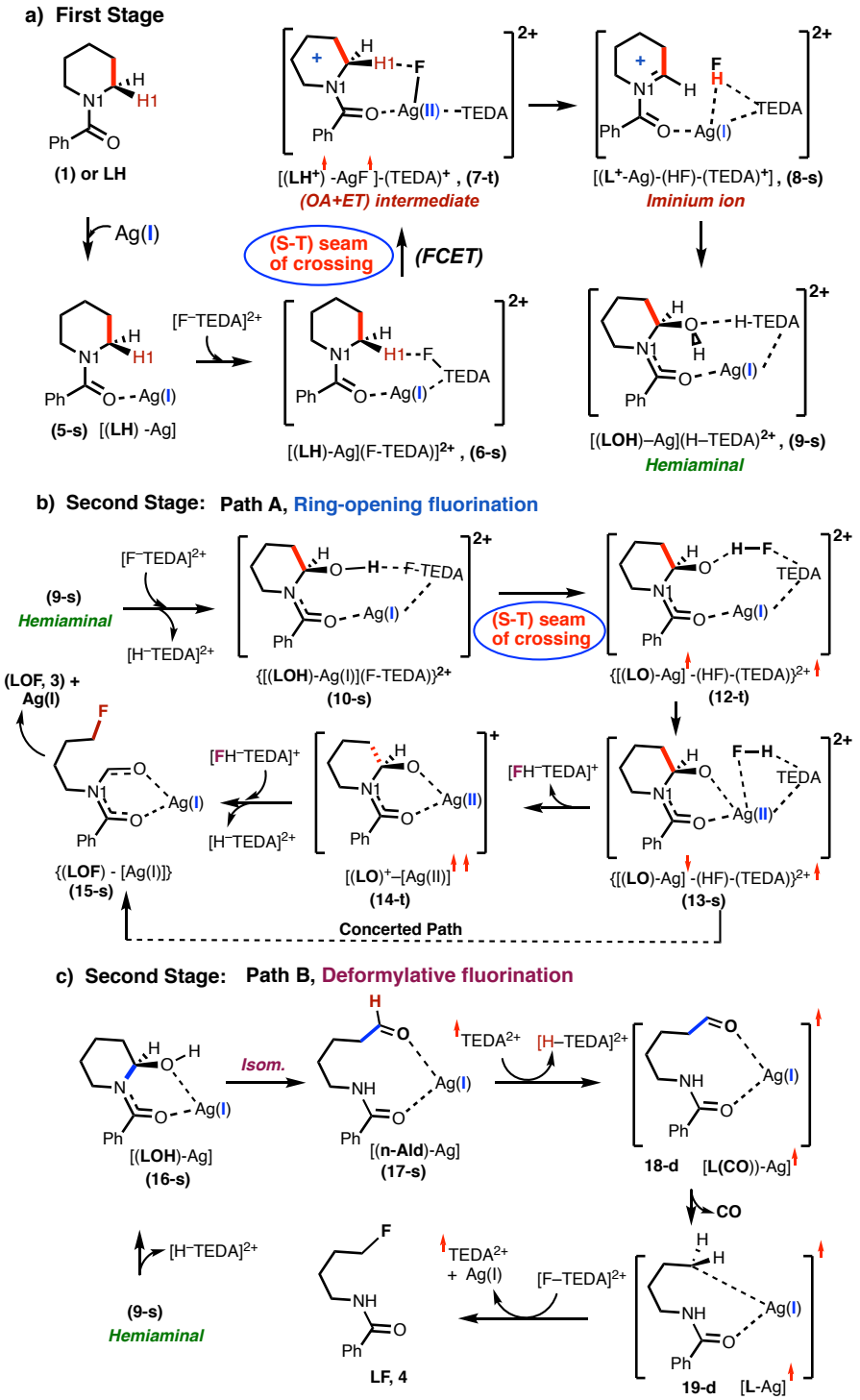

Scheme 2. Previously proposed mechanism of the Silver(I)-mediated deconstructive fluorination of *N*-protected cyclic amine **1** (or **LH**) by using the commercially available N–F reagent Selectfluor® (**2**;(F–TEDA)$^{2+}$) [see also, ref. 86]

In order to design less expensive reagents and conditions that will serve as alternatives to the Ag(I)-mediated deconstructive fluorination [83-86], here, we investigate the mechanism of the analogous reaction with Cu(I) at the density functional level of theory (DFT). Our calculations show that (a) coordination of substrate to Cu(I), which is the first step, is important for the overall process, and (b) iminium ion formation occurs through a *two-state reactivity* (*TSR*) process here as well, proceeding via a F-atom coupled electron transfer (FCET) to give the oxidative addition

coupled electron transfer (*OA+ET*) product. The C–C cleavage/fluorination of the hemiaminal is also calculated to be a *two-state reactivity (TSR)* event. Compared with the Ag(I)-mediated process, for the Cu(I) reaction (a) the iminium ion formation and hemiaminal fluorination have lower associated energy barriers, whereas the (b) product release and catalyst regeneration steps have higher energy barriers.

Computational Details

All reported computational results were obtained using the Gaussian-16 suite of programs [111] at the B3LYP-D3(BJ)/[6-31G(d,p) + Lanl2dz (Cu and Ag)] level of theory with the corresponding Hay-Wadt effective core potential [112-114] for Cu and Ag. In the calculations described here, we used the B3LYP density functional [115-117] with Grimme's empirical dispersion-correction (D3) [118] and Becke-Johnson (BJ) damping-correction [119-121]. Frequency analyses were used to characterize each minimum and transition state (TS) with zero and one imaginary frequency, respectively. Intrinsic reaction coordinate (IRC) calculations were performed for all TSs to ensure their true nature. Singlet-triplet interactions were characterized by minimizing the energy of singlet-triplet (i.e. S0/T1) seams of crossing (**MSX**). Singlet-(open-shell-singlet) (i.e., S0/S1) conical intersections (**CX**) were estimated as single point energy calculations of the open-shell singlet at the located MSX geometries. The MSX calculations were performed with the mecpro-1.0.3 suite of codes [122]. Bulk solvent effects were incorporated for all calculations (including geometry optimizations and frequency calculations) using the self-consistent reaction field polarizable continuum model (IEF-PCM) [123,124]. We chose water as solvent. The reported thermodynamic data were computed at a temperature of 298.15 K and at 1 atm of pressure. Various spin states (including the open-shell singlet states, where that is appropriate) were considered for all key species. Unless otherwise stated, energies are given as ΔH/ΔG in kcal/mol.

Here, as in our previous report [86], we use dication $[F\text{-}TEDA]^{2+}$ as a model for Selectfluor®. We use "**X-y-M**" labeling to denote calculated structures, where **X** is a number associated with the reported structure, and **y** is assigned for the singlet (**s**), doublet (**d**), or triplet (**t**) states of the calculated structures, and **M** denotes Cu or Ag.

In order to validate the [B3LYP-D3(BJ)+PCM]/[6-31G(d,p) + Lanl2dz(Cu)] basis set in this study, we have also performed a series of calculations at the highest possible levels of theory for the important steps of the reported potential energy surfaces. Specifically, the formation of a [(**LH**)-Cu(I)] intermediate from **LH** and $CuBF_4$, F-atom abstraction by Cu(I) and [(**LH**)-Cu(I)] from $F\text{–}TEDA^{2+}$, and the energy of the **6-s-Cu → 7b-t-Cu** and **10-s-Cu → 11-t-Cu** transformations were re-calculated at the [B3LYP-D3(BJ)+PCM]/[cc-pVTZ + Lanl2dz(f)(Cu)] [125] (to validate the basis sets), and [wB97XD+PCM]/[cc-pVTZ + Lanl2dz(f)(Cu)] [126] level (to validate the B3LYP density functional). Results of these calculations are given in the Supporting Information (see Table S1), and in the main text where that is appropriate. We found that changing the basis sets from [6-31G(d,p) + Lanl2dz(Cu)] to [cc-pVTZ + Lanl2dz(f)(Cu)], as well as the density functional (from B3LYP-D3(BJ) to wB97XD) resulted in only a few kcal/mol change in the calculated energies and does not impact our main conclusions.

Results and Discussion

For the starting substrate (**LH**), in the presence of $CuBF_4$ (denoted as Cu(I), below), and Selectfluor (**2)** (modeled as $[F\text{–}TEDA]^{2+}$) [127] reaction of either **LH** or $[F\text{-}TEDA]^{2+}$ with Cu(I) is anticipated. Previous experiments [83-85] have established that no reaction occurs between **LH** and $[F\text{-}TEDA]^{2+}$. On the basis of a seminal report by Lectka and coworkers, [80] Cu(I) and $[F\text{-}TEDA]^{2+}$ may react via a fluorine abstraction pathway, leading to a FCu(II) intermediate and a $TEDA^{2+}$ dicationic radical. Our calculations (see Figure 1) show that the reaction:

$$Cu(I) + [F\text{-}TEDA]^{2+} \rightarrow Cu(I)[F\text{-}TEDA]^{2+} \rightarrow FCu(II) + TEDA^{2+} \qquad \text{(Eq. 1)}$$

is only slightly exergonic (by 1.6/2.6 kcal/mol; relative to the reactants), and intermediate $Cu(I)[F\text{-}TEDA]^{2+}$ has a small complexation energy of 12.3/0.7 kcal/mol. A competing reaction pathway is the dimerization of the putative FCu(II) species, a process which has been calculated to be highly exergonic (by 52.7/39.7 kcal/mol). However, this dimerization is not expected to impact the $TEDA^{2+}$ radical formation process [128]. Although, Musaev, Itami, and coworkers showed both experimentally [78] and computationally [79] that the dimer $[LCu(II)F]_2$ forms during the (6,6'-Me_2bpy)Cu(I)-catalyzed C–H imidation of arenes, a different N–F reagent (NFSI) was used. Therefore, the most important factor impacting the outcome of the fluorine abstraction reaction (Eq. 1) is the energy barrier at the minimum of the singlet-triplet seam of crossing (**MSX**) as well as the conical intersection (CX) region of the S0/S1. Our DFT calculations indicate that the MSX and CX energy barriers are about 17.4 and 8.1 kcal/mol, respectively, higher

relative to the singlet minimum, and the activated F–TEDA and forming Cu–F bond distances at the **MSX** are 1.82 and 1.83 Å, respectively (see Figure S1 in the Supporting Information). Since **MSX** is not a true stationary point on the potential energy surface, below we will report only the ΔE values for the barrier associated with the **MSX** structures.

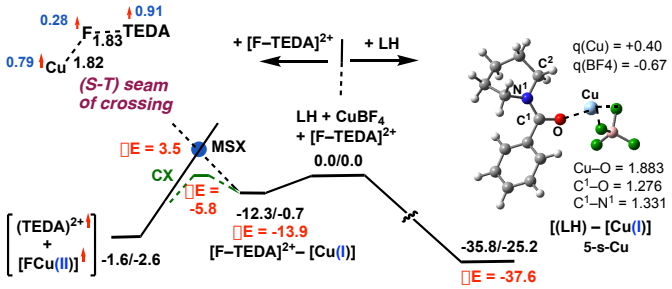

Figure 1. Schematic presentation of energy profiles of the F-atom abstraction (left), and the **LH** coordination (right) pathways of the reaction **LH** + **Cu(I)** + $[F–TEDA]^{2+}$. The relative energies are given as ΔH/ΔG, in kcal/mol. Here, **MSX** represents the minimum of the S0/T1 curve crossing, and **CX** represents the S0/S1 conical intersections. See the Supporting Information for geometries of the presented structures.

Along the reaction coordinate, the fluorine abstraction is calculated to be disfavored on kinetic grounds than coordination of **LH** to Cu(I), i.e. the formation of singlet state adduct [(**LH**)–Cu(I)], **5-s-Cu**, (see Figure 1), which is calculated to be exergonic [129] by 35.8/25.2 kcal/mol and proceeds with no energy barrier. A charge density analysis (see the Supporting Information) indicates that in **5-s-Cu**, 0.27 |e| charge is transferred from **LH** to Cu(I). Comparison of the calculated data for [(**LH**)–Cu(I)] with those for the [(**LH**)–Ag(I)] analog [86], shows that: (a) the Cu(I)–**LH** interaction is stronger than the analogous Ag(I)–**LH** interaction, and (b) substrate **LH** is oxidized to a larger extent in [(**LH**)–Cu(I)] than in [(**LH**)–Ag(I)]. This is likely the result of the less positive Cu(I)/Cu(0) redox potential (+0.52 eV vs SHE) compared to the Ag(I)/Ag(0) potential (+0.80 eV SHE) [130].

On the basis of our computations, the reaction mixture of **LH**, $CuBF_4$, and Selectfluor®, is expected to lead to adduct **5-s-Cu**, if equimolar quantities of substrate **LH** and Cu(I) salt are employed. In other words, iminium-ion formation is expected through the reaction of **5-s-Cu** with **2** (Selectfluor®). Notably, this conclusion differs from that reached in the seminal paper by Lectka and coworkers [80]. In their study of a Cu(I)-promoted C–H fluorination of aliphatic substrates, Lectka and coworkers concluded that in the fluorination of an aliphatic substrate by the combination of Cu(I) and Selectfluor®, the reaction proceeds by (a) F-atom abstraction by Cu(I) and $TEDA^{2+}$ radical formation, (b) C–H bond abstraction from the alkyl substrate by the $TEDA^{2+}$ radical, and (c) C-radical fluorination by another equivalent of $[F–TEDA]^{2+}$. This difference between our conclusion (i.e., initial coordination of Cu(I) to the amide substrate, **LH**) and that reached by Lectka and coworkers (direct reaction of Cu(I) with Selectfluor®) likely arises due to the difference in substrates examined. In our case, cyclic amine **LH** bears an amide carbonyl group which binds strongly to the Cu(I)-center and initiates partial reduction of Cu(I). On the other hand, Lectka and coworkers used aliphatic substrates which could not bind the Cu(I) center. *Therefore, the electronics and functional groups of the substrate are important contributors to the reaction path.* However, in line with the report from Lectka and co-workers, we cannot rule out the alternative pathway that starts with the generation of a $TEDA^{2+}$ radical followed by α-C–H abstraction.

Mechanism of the Iminium-ion formation.

Interaction of **5-s-Cu** with $(F\text{-}TEDA)^{2+}$ results in a meta-stable complex [(**LH**)-Cu(I)]–$[F\text{-}TEDA]^{2+}$ (**6-s-Cu**) in the singlet ground electronic state (see Figure 2, and the Supporting Information). The calculated complexation energy of the reaction

[(**LH**)-Cu(I)], **5-s-Cu** + $[F\text{-}TEDA]^{2+}$ → [(**LH**)-Cu(I)]–$[F\text{-}TEDA]^{2+}$ (**6-s-Cu**)

is only 16.6/2.9 kcal/mol. From **6-s-Cu** the reaction may proceed via two competing pathways involving either (a) a F-atom abstraction by [(**LH**)-Cu(I)] to form triplet state complex [(**LH**)-Cu(II)F]·–$TEDA^{2+\cdot}$, **7a-t-Cu**, or (b) a N–F oxidative addition coupled with electron transfer (*OA+ET*), as proposed in the previously reported Ag(I)-mediated reaction [86]. Our calculations indicate that F-atom abstraction by [(**LH**)-Cu(I)], (i.e., Eq. 2)

(6-s-Cu) → MSX-1-Cu → (7a-t-Cu) (Eq. 2)

is exergonic by 4.6/4.4 kcal/mol and has a barrier of 10.7 and 6.1 kcal/mol, respectively (at the minimum of the singlet-triplet seam of crossing, **MSX-1-Cu,** and at the corresponding S0/S1 conical intersection). On the basis of the calculated spin density and charge analyses (see Figure 3), complex **7a-t-Cu** was characterized as a triplet state complex [(**LH**)-FCu(II)]·–TEDA$^{2+\cdot}$ with one unpaired electron located on the CuF and one unpaired electron on the [TEDA^{2+}] fragment. Its open-shell singlet electronic state is just 0.2 kcal/mol higher in free energy.

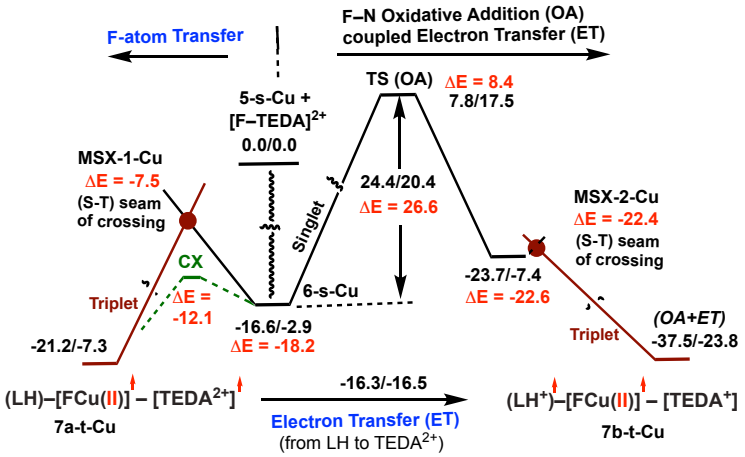

Figure 2. Energy profiles of the F-atom abstraction coupled electron transfer (left), and the N–F oxidative addition coupled electron transfer (*OA+ET*, right) pathways of the reaction **5-s-Cu** + [F–TEDA]$^{2+}$ → [(**LH**$^{+}$)·-(CuF)·–(TEDA)$^{+}$], (**7b-t-Cu**). The relative energies are given as ΔH/ΔG, in kcal/mol. Here, **MSX** represents the minimum of the S0/T1 crossing, and **CX** represents the S0/S1 conical intersection. See Figure 3 for the important structural and electronic parameters of critical points along these potential energy profiles.

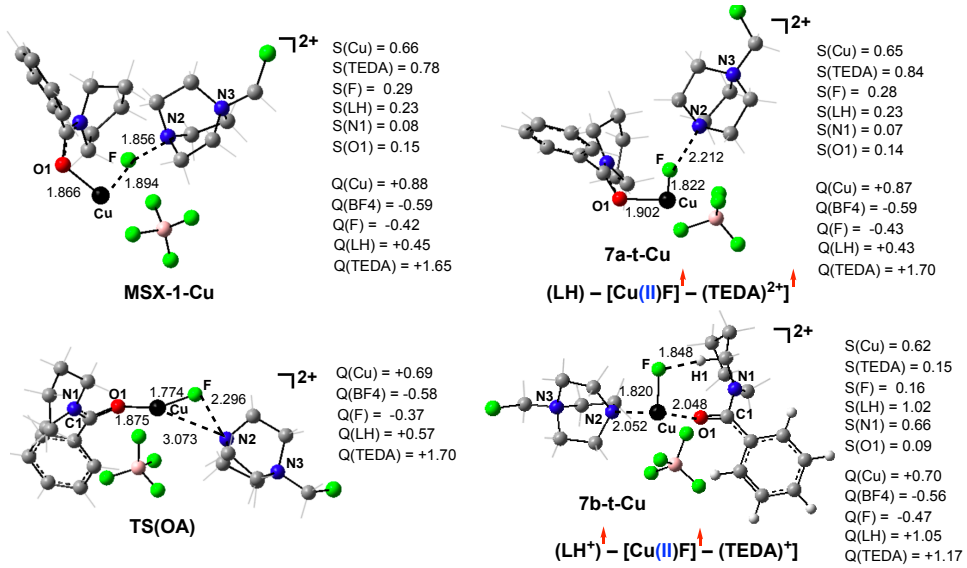

Figure 3. The calculated structures of the **MSX-1-Cu**, oxidative addition (OA) transition state **TS (OA)**, intermediates **7a-t-Cu** and **7b-t-Cu** alone with their important geometry parameters (in Å), Mulliken charges (Q, in |e|) and spin densities (S, in |e|).

The pathway leading to the oxidative addition coupled with electron transfer (*OA+ET*) product, i.e., triplet state complex [(**LH**$^{+}$)·-(CuF)·–(TEDA)$^{+}$] (**7b-t-Cu**), while highly exergonic (by 20.9/20.9 kcal/mol), has a calculated energy barrier of 24.4/20.4 kcal/mol (26.6 kcal/mol, at the electronic energy level), at the singlet state oxidative

addition transition state **TS(OA)** relative to intermediate **6-s-Cu**. Detailed analyses (see Figure 3) show that in complex **7b-t-Cu**, **LH** is oxidized by 1-electron, which has transferred to the TEDA-fragment. Therefore, two unpaired spins are localized in the oxidized substrate ($\mathbf{LH}^+$) and CuF-units. The overall reaction

$$[(\mathbf{LH})\text{-Cu(I)}] + [\text{F-TEDA}]^{2+}] \rightarrow [(\mathbf{LH}^+)^{\cdot}\text{-(CuF)}^{\cdot}\text{–(TEDA)}^+], (\mathbf{7b\text{-}t\text{-}Cu}) \qquad \text{Eq. (3)}$$

is calculated to be exergonic by 37.5/23.8 kcal/mol. Employing more rigorous levels of theory do not significantly alter the calculated energy values. For example, at the [B3LYP-D3(BJ)+PCM]/[cc-pVTZ + Lanl2dz(f)(Cu)] and [wB97XD+PCM]/[cc-pVTZ + Lanl2dz(f)(Cu)] levels of theory, values for the exergonic nature of Eq. 3 are 35.0/21.2 and 33.3/22.7 kcal/mol, respectively.

Our calculations up to this stage point to a *two-state reactivity* (*TSR*) event for N–F addition to the [(**LH**)–(Cu(I)] adduct that starts from a F-atom abstraction by the Cu(I)-center at the minimum of the singlet-to-triplet seam of crossing (**MSX-1-Cu**), involving the lower lying S0/S1 **CX**. This is followed by electron transfer (from **LH** to a $TEDA^{2+}$ radical dication) to form a product, [$(\mathbf{LH}^+)^{\cdot}$–$(CuF)^{\cdot}$–$(TEDA)^+$], **7b-t-Cu**, that is formally the outcome of an oxidative addition coupled electron transfer (*OA+ET*). Direct formation of **7b-t-Cu** requires a much higher energy barrier at the transition state **TS(OA)** and is, therefore, kinetically unlikely.

Our comparison of the Cu(I)-, and the previously reported Ag(I)-mediated deconstructive fluorination shows that the transition metal impacts the reaction path. As seen in a comparison of Figures 2 and 4, the Cu(I)-mediated **6-s-Cu** → **7b-t-Cu** transition has a lower barrier compared to the Ag(I)-mediated **6-s-Ag** → **7b-t-Ag** transition. Indeed, the former has a 10.7 kcal/mol barrier for the F-atom transfer at the **MSX-1-Cu** (and 6.1 kcal/mol at the S0/S1 **CX**) and is exergonic by 20.9/20.9 kcal/mol. In contrast, the **6-s-Ag** → **7b-t-Ag** transition has a barrier of 30.1 kcal/mol for the F-atom transfer at the minimum of the singlet-to-triplet seam of crossing **MSX-1-Ag**, and 25.5 kcal/mol via the S0/S1 **CX**, and is endergonic by 13.4/13.5 kcal/mol. The calculated difference in energies of the Cu(I)- and Ag(I)-mediated F-atom transfer coupled electron transfer (*OA+ET*) leading to **7b-t** can be mostly explained by the difference in the Cu(I)/Cu(II) and Ag(I)/Ag(II) redox potentials, which are +0.159 and +1.98 eV SHE, respectively [130]. These changes also correlate with the calculated geometry of the MSX structures: in **MSX-1-Cu** the calculated F-TEDA bond distance (1.856 Å) is shorter than in the **MSX-1-Ag** (1.941 Å: see Figure 3 and the Supporting information).

From intermediate **7b-t-Cu**, as in the Ag(I)-mediated process [86], H–F bond formation via hydrogen atom tranfer leads to the iminium ion complex **8-s-Cu**, [$\mathbf{L}^+$-Cu]–(FH)–[$TEDA^+$], in the ground singlet state (see Figure 5). Our calculations show that the **7-t-Cu** → **8-s-Cu** transformation is (a) exergonic by 38.7/40.3 kcal/mol and occurs through an almost barrierless H–F bond formation (in the case of the Ag(I)-mediated process, this energy barrier was calculated to be 1.4/1.5 kcal/mol), [86].

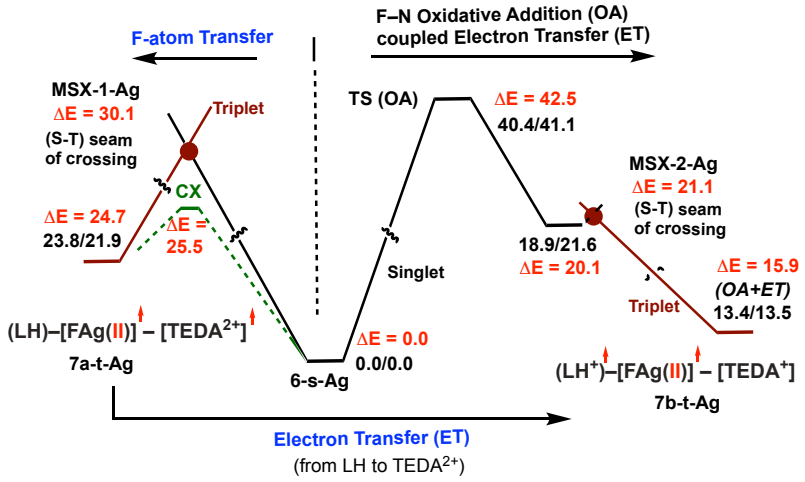

Figure 4. Energy profiles of the F-atom abstraction coupled electron transfer (left), and the N–F oxidative addition coupled electron transfer (*OA+ET*, right) pathways of the reaction **6-s-Ag** → [$(\mathbf{LH}^+)^{\cdot}$-$(AgF)^{\cdot}$–$(TEDA)^+$] (**7b-t-Ag**). The relative energies are given as ΔH/ΔG, in kcal/mol.

The conversion of iminium ion complex **8-s-Cu** to hemiaminal complex **9-s-Cu** is anticipated to proceed with a very low energy barrier (see Figure 5). As shown previously, this occurs via HF → H_2O exchange, deprotonation of the metal-bound water by monocationic $TEDA^+$, and a subsequent C2–OH bond formation [86]. The overall process **8-s-Cu** + H_2O → **9-s-Cu** + HF is exergonic by –2.5/-1.2 kcal/mol. The resultant **9-s-Cu** is a Cu(I) complex, [(**LOH**)-Cu(I)](H-TEDA)$^{2+}$ (see Figure 5, and the Supporting Information).

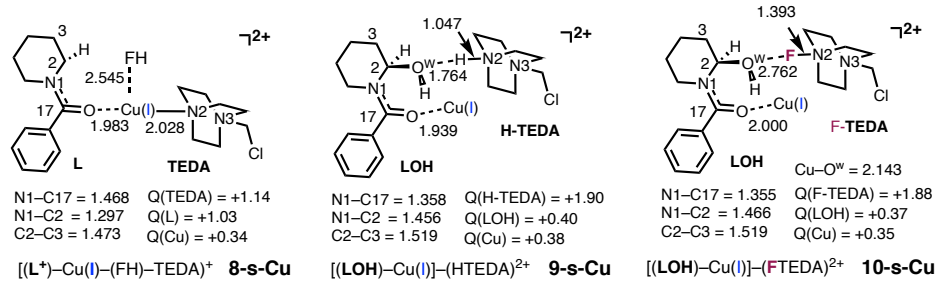

Figure 5. Calculated iminium-ion, **8-s-Cu,** hemiaminal **9-s-Cu** and **10-s-Cu** complexes, along with their important geometry and electronic parameters (distances are in Å, and Mulliken charges, **Q**, are in |e|)). See also the Supporting Information.

C. Fluorination of hemiaminal complex 9-s-Cu. Hemiaminal **LOH** is converted to the final fluorinated products **LOF** or/and **LF** (see Scheme 1) under the Ag(I)-mediated conditions. As shown previously, this can occur via "ring-opening" (Path-A, Scheme 2b) or "deformylative" (Path-B, Scheme 2c) fluorination mechanisms [83-86]. One of the factors impacting the selectivity of the radical ring opening pathway depicted in pathway A (i.e., C–N vs C–C cleavage) is the difference between the bond dissociation energies (BDEs) of the C2–C3 and N–C2 bonds. Here, we discuss only enthalpy (ΔH) values of the calculated BDEs. The details of these calculations are described in Figure S2 in the Supporting Information. The calculated BDEs of the N–C2 and C2–C3 bonds are 74.2 and 73.2 kcal/mol, respectively in **LOH**. Complexation of **LOH** with $AgBF_4$ leads only to small changes in the values of the calculated BDE's: in [(**LOH**)-Ag] adduct the N–C2 and C2–C3 BDEs are 74.2 and 72.3 kcal/mol, respectively. These small changes correlate with a computed weak interaction between hemiaminal **LOH** and $AgBF_4$, which nonetheless makes the cleavage of C2–C3 slightly more favorable compared to N–C2 cleavage.

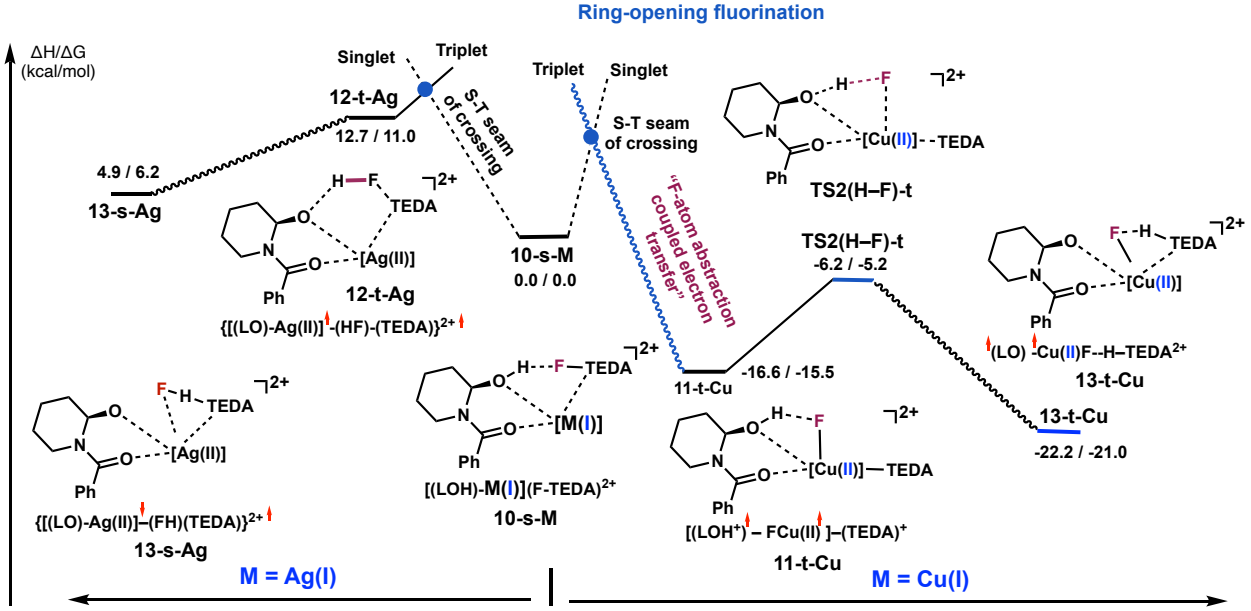

Figure 6. Schematic comparison of the (S–T) seam of crossing, oxidative addition coupled with electron transfer (*OA+ET*), and H–F bond formation steps of the Ag(I) (left) and Cu(I) (right) mediated ring-opening fluorination of the hemiaminal.

In contrast, in adduct [(**LOH**)-Cu], a strong interaction between the hemiaminal **LOH** and $CuBF_4$ was calculated. In this case, the calculated N–C2 and C2–C3 BDEs are significantly smaller (48.6 and 20.1 kcal/mol, respectively). Therefore, in [(**LOH**)-Cu], a facile fluorination of both N–C2 and C2–C3 is anticipated. However, higher selectivity for C3-fluorination is expected as compared to the [(**LOH**)-Ag] case.

C.1. Ring-opening fluorination of hemiaminal (Path A). As shown previously by us [86], Path-A begins with an $(H\text{-}TEDA)^{2+} \rightarrow (F\text{-}TEDA)^{2+}$ exchange in **9-s**. This step has a lower barrier for the Cu(I)- as compared to the Ag(I)-mediated process. Indeed, we find that intermediate **10-s-Cu** (i.e., [(**LOH**)-Cu](F–TEDA)$^{2+}$, is only 5.0/4.1 kcal/mol higher in energy than **9-s-Cu**, and the **9-s-Cu → 10-s-Cu** transformation requires only by 6.5 kcal/mol free energy barrier (for more details see Figure 5, and Figure S3 in the Supporting Information). In the Ag(I)-mediated case, this process was reported to be endergonic by 5.2 kcal/mol and required by 10.3 kcal/mol free energy barrier [86]. Regardless, in both cases, this step of the reaction has a lower barrier and is unlikely to impact the outcome of the overall "ring-opening" fluorination of hemiaminal **LOH**.

The next step of the ring-opening fluorination of hemiaminal **10-s** is more facile for the Cu(I)-mediated reaction than the Ag(I)-mediated one, and proceeds via a conceptually different mechanism (see Figure 6). In the case of M = Ag, this step is a concerted F-atom and H-atom coupling (i.e., direct H–F bond formation) event that occurs via the *two-state reactivity* (*TSR*) scenario, has a 11.0 kcal/mol of free energy activation, and leads to the diradical alkoxide intermediate [(**LO**)-Ag(II)]$^{\bullet}$–(HF)–$(TEDA)^{2+\bullet}$ **12-t-Ag**. In **12-t-Ag** dicationic $TEDA^{2+}$ and [(**LO**)-Ag] units each possess almost one unpaired electron. This intermediate is meta-stable and isomerizes to the energetically most stable open-shell singlet intermediate $\{[(\mathbf{LO})^{\bullet}\text{-Ag(II)}^{\bullet}]\text{–(FH)–(TEDA)}\}^{2+}$, **13-s-Ag**. In contrast, when M = Cu, the process is initiated from **10-s-Cu** and is a F-atom abstraction followed by an electron transfer event that leads to the triplet state, formally, oxidative addition coupled electron transfer (*OA+ET*) product $[(\mathbf{LOH}^{+})^{\bullet}\text{–FCu(II)}]^{\bullet}\text{–(TEDA)}^{+}$, **11-t-Cu.**

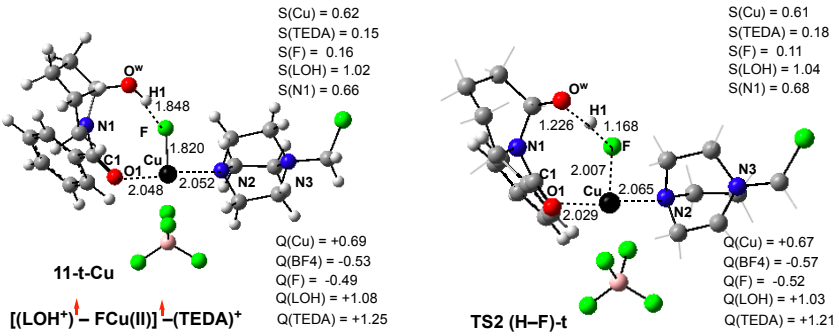

Figure 7. The calculated *OA+ET* complex, $[(\mathbf{LOH}^{+})^{\bullet}\text{–FCu(II)}]^{\bullet}\text{–(TEDA)}^{+}$, **11-t-Cu**, and the following H–F bond formation transition state **TS2(H–F)-t** with their important geometry and electronic parameters, The geometries of the presented structures are in Å, and their charge (Q) and spin (S) densities are in |e|.

This step of the reaction is a *two-state reactivity* (*TSR*) event, and should theoretically occur via similar intermediates and transition states as those presented for the **6-s-Cu → 7b-t-Cu** transition. In fact, the electronic structure of the product complex (**11-t-Cu**) is similar to that of the **7b-t-Cu** intermediate (discussed above in Figure 3). Indeed, in **11-t-Cu,** as in **7b-t-Cu**, two unpaired spins are located mostly in the ligand (i.e., **LOH)** and CuF fragments (see Figure 7).

The subsequent H–F bond formation in **11-t-Cu** was calculated to be a proton/fluoride coupling event triggered by an electron transfer from the $TEDA^{+}$ fragment to the CuF-unit. It proceeds via the H–F formation transition state **TS2(H-F)-**t (see Figure 7). This complex has a triplet ground state (its open-shell singlet state is only 0.06/0.6 kcal/mol higher in free energy) and leads to **12-t-Cu** (see Figure 8). Spin density and charge analyses show that intermediate **12-t-Cu** is a [(**LO**)–Cu(II)]$^{\bullet}$–(HF)–$(TEDA)^{2+\bullet}$ species. Thus, in this intermediate, like in the previously reported **12-t-**

Ag intermediate, dicationic $[TEDA]^{2+}$ and [(**LO**)-Cu] units each possess almost one unpaired electron. However, this intermediate is meta-stable and isomerizes to the energetically most stable triplet state intermediate $\{[(\mathbf{LO})^{\bullet}\text{-Cu(II)}^{\bullet}]\text{–(FH)–(TEDA)}\}^{2+}$, **13-t-Cu**. As seen in Figure 8, in intermediate **13-t-Cu** two unpaired α-spins are located in the [(**LO**)-Cu] unit and distributed as 1.20 |e| and 0.65 |e| in the **LO** and Cu, respectively. Interestingly, the FH–$TEDA^{2+}$ fragment of **13-t-Cu** can be best represented as zwitterionic structure F^{-}–$(HTEDA)^{2+}$.

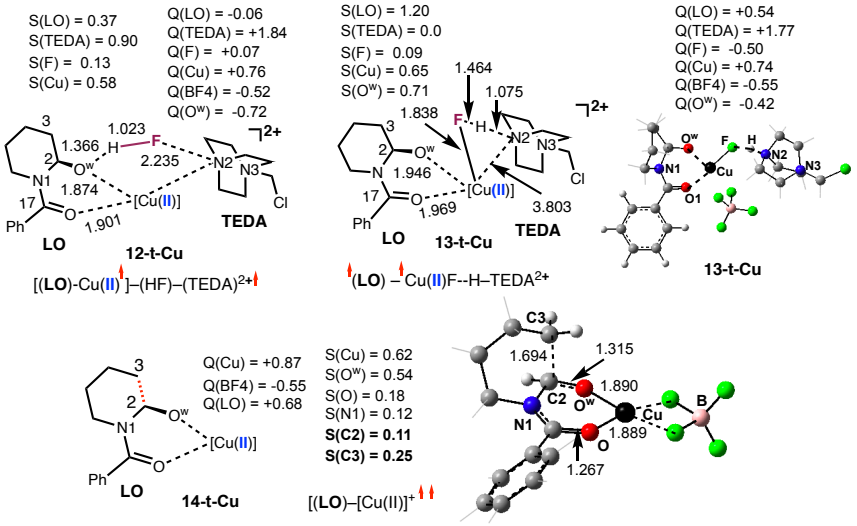

Figure 8. The calculated geometries (in Å), charge (Q) and spin (S) densities (in |e|) of the complexes $[(\mathbf{LO})\text{–Cu(II)}^{\bullet}]\text{–(HF)–(TEDA)}^{2+\bullet}$, **12-t-Cu**, $[(\mathbf{LO})^{\bullet}\text{–Cu(II)}^{\bullet}]\text{–(FH)–(TEDA)}^{2+}$, **13-t-Cu**, and $[(\mathbf{LO})\text{–Cu(II)}]^{+\bullet\bullet}$, **14-t-Cu**.

Conversion of alkoxide intermediate **13-t-Cu** to the alkyl fluoride product (i.e., **LOF**, or **3**, see Scheme 1), as also shown previously for the Ag-systems [86], is a multi-component process. It may occur through several competing pathways (see Scheme 4). Path-1 (stepwise) and path-2 (concerted) engage the HF by-product as a fluoride source, while path-3 utilizes another equivalent of Selectfluor®. As we have shown previously [86], the analyses of the reactions

$$\{[(\mathbf{LO})\text{-Cu}]\text{–(HF)–(TEDA)}\}^{2+}\ (\mathbf{13\text{-}t\text{-}Cu}) \rightarrow \{[(\mathbf{LO})\text{-Cu}] + [(FH)\text{–TEDA}]^{2+} \qquad \text{(Eq. 3)}$$

and

$$\{[(\mathbf{LO})\text{-Cu}]\text{–(HF)–(TEDA)}\}^{2+}\ (\mathbf{13\text{-}t\text{-}Cu}) \rightarrow \{[(\mathbf{LO})\text{-Cu}]^{+}\ (\mathbf{14\text{-}t\text{-}Cu}) + [(FH)\text{–TEDA}]^{+} \qquad \text{(Eq. 4)}$$

provide insight into the nature of the **13-t-Cu** conversion to the final alkyl fluoride product **LOF**. Here, we found that the reaction depicted in Eq. 3 is thermodynamically less favorable than the reaction in Eq. 4 (see Figure S4 in the Supporting Information). Therefore, we only discuss the reaction depicted in Eq. 4 (path-1 in Scheme 4), which has a barrier of 34.9/20.5 kcal/mol associated with formation of the triplet state complex $[(\mathbf{LO})\text{-Cu}]^{+}$ (**14-t-Cu**) (see Figures 8, and Scheme 4). Spin density and charge analyses show that in intermediate **14-t-Cu**, the Cu-center has 0.62 |e| of unpaired α-spin, and, critically, the C2 and C3 centers have also acquired additional unpaired α-spins (0.11 and 0.25 |e|, respectively). This spin distribution is consistent with a significant elongation (by 0.148 Å) of the C2–C3 bond distance. A similar effect was previously reported for the Ag-mediated reaction [86], but it is more pronounced for the Cu-system, which is consistent with the (smaller) calculated C2–C3 BDEs in [(**LOH**)-Cu] than [(**LOH**)-Ag] adducts. The C3-center in **14-t-Cu** is well suited to coordinate $[(FH)\text{–TEDA}]^{+}$ and initiate heterolytic cleavage of HF leading to formation of the [(**LOF**)-Cu(I)], **15-s-Cu**, and the $[H\text{–TEDA}]^{2+}$ dication. *Therefore, the oxidation of the **LO** unit (a result of a stronger Cu-**LOH** interaction) is critical for the facile selective C2–C3 cleavage/ fluorination of the N-protected cyclic amine **LH**.*

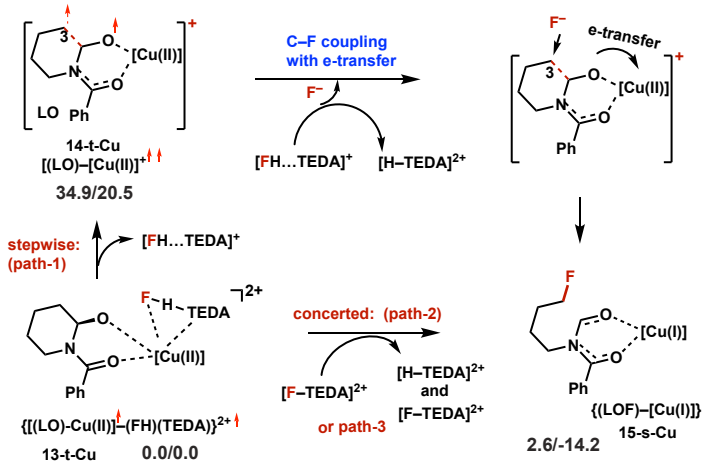

Scheme 4. Schematic presentation of elementary reactions involved in the **13-t** → [(**LOF**)–[Cu(I)], **15-s-Cu**, transformation.

As anticipated, the reaction **14-t-Cu** + $[(FH)–TEDA]^+$ → **15-s-Cu** + $[H–TEDA]^{2+}$ is highly exergonic (by 32.3/34.7 kcal/mol). However, it may require additional energy to overcome the minimum of the triplet-singlet seam of crossing, which is not reported in this paper, because we anticipate that path-1 will not compete with path-2 or path-3. The pathways that follow are exergonic by 14.2 kcal/mol and are expected to proceed with smaller energy barriers for the fluoride–C3 coupling. Notably, a mechanism involving electron transfer followed by fluoride trapping by the nascent cation (path-2) was previously postulated by Sammis and co-workers [81].

The dissociation of Cu(I) from [(**LOF**)–Cu(I)] completes the formation of fluorinated product **LOF** (**3**). This step is endergonic by 25.2 kcal/mol, and is calculated to be the highest energy demanding step of the entire Cu(I)-mediated deconstructive fluorination process**.** In contrast, in the analogous Ag(I)-mediated reaction, this step was calculated to be endergonic by only 5.8 kcal/mol [86].

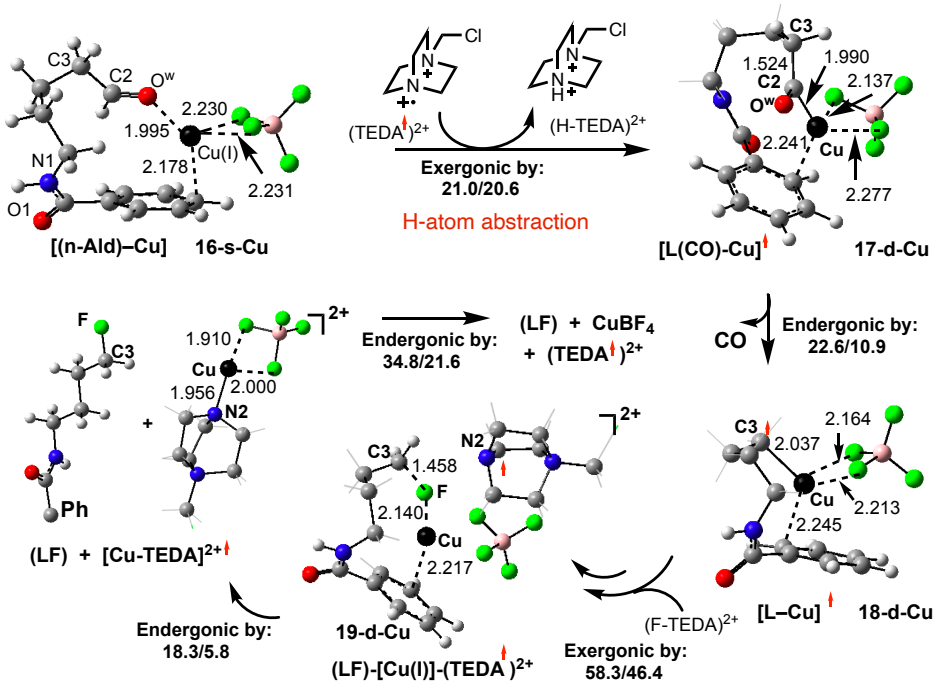

Figure 8. Calculated representative structures, along with their key geometry parameters (distances are in Å), of the proposed mechanism for the deformylative fluorination by Selectfluor®. Energies (in kcal/mol) are provided relative to pre-reaction complex as ΔH/ΔG.

C.2. Deformylative fluorination of hemiaminal (Path-B). The alternative "deformylative" C2–C3 bond cleavage/fluorination pathway also starts from hemiaminal complex {[(**LOH**)-Cu](H–TEDA)}$^{2+}$, **9-s-Cu**, but is initiated by equilibration of the hemiaminal (**LOH**) to the corresponding aldehyde (**Ald**). This hemiaminal to aldehyde transformation may occur either directly from **9-s-Cu,** or following dissociation of [H–TEDA]$^{2+}$, or via a metal-free **LOH** → **Ald** equilibration. While we have previously stressed that calculations alone cannot unambiguously distinguish these possibilities [86], we have now calculated that the conversion of (**LOH**) to linear aldehyde (**l-Ald**) is exergonic by 6.0 kcal/mol in the absence of other coordinating groups, but endergonic by 2.2 kcal/mol for the Cu-coordinated hemiaminal (see the Supporting Information). We have identified several lower energy isomers of the [(**Ald)**-Cu] complex (see also Figure S5 in the Supporting Information), and use the lowest energy complex **16-s-Cu** as an initial point for calculations of the "deformylative" fluorination process. As previously demonstrated by us [86], this multistep process involves a formyl H-atom abstraction by a TEDA^{2+} radical dication, decarbonylation, and fluorination of the C3-radical center by another equivalent of Selectfluor® steps.

In the current study, we examined the same mechanistic steps (see Figure 8) and found that a formyl H-atom abstraction by [TEDA]$^{2+}$ radical dication from **16-s-Cu** is exergonic by 21.0/20.6 kcal/mol and proceeds without free energy barrier (the calculated energy barrier at the enthalpy level is only 1.2 kcal/mol, see Figure S7 of the Supporting Information).The resulting intermediate, **17-d-Cu**, has one unpaired α-spin delocalized at C2 (0.30 |e|), C3 (0.13 |e|), Cu (0.21 |e|), and O (0.34 |e|). The subsequent decarbonylation from **17-d-Cu** is endergonic by only 10.9 kcal/mol and leads to another radical intermediate [**L**-Cu], **18-d-Cu**, which upon reaction with another equivalent of Selectfluor® completes fluorination of the C3-center. This step of the reaction is highly exergonic (by 58.3/46.4 kcal/mol). As in the "ring-opening" fluorination pathway discussed above, the crucial step of the "deformylative" fluorination is also the product-releasing and catalyst-regeneration step, i.e. reaction **19-d-Cu** → **LF** + [Cu-TEDA]$^{2+}$ → **LF** + Cu(I) + [TEDA]$^{2+}$, which is endergonic by 27.4 kcal/mol. This energy value is comparable to the 25.2 kcal/mol for the product-release step of the ring-opening pathway.

Conclusions

The computational studies and analyses presented here lead us to conclude that the Cu(I)-mediated deconstructive fluorination of an *N*-benzoylated cyclic amine (**LH**) by Selectfluor® proceeds via: (a) substrate coordination, (b) iminium ion formation followed by transformation to a hemiaminal species, and (c) hemiaminal fluorination.

1. Coordination of the amide substrate to the Cu center, occurs in a first step of the reaction.
2. Iminium ion formation from the [(**LH**)–(Cu(I)] adduct and Selectfluor® proceeds through F-atom coupled electron transfer (FCET) mechanism to form, formally, an oxidative addition coupled electron transfer (*OA+ET*) product [(**LH**$^{+}$)·–(CuF)·–(TEDA)$^{+}$], **7b-t-Cu**.
3. Fluorination of the hemiaminal intermediate may occur via either ring-opening or deformylative fluorination pathways. A ring-opening fluorination (i.e., via β-C–C cleavage/fluorination) is a *two-state reactivity (TSR)* event. However, a competing deformylative fluorination initiated by a hemiaminal to aldehyde equilibration, followed by H-atom abstraction by a TEDA^{2+} radical dication from the formyl group, decarbonylation, and fluorination of the C3-radical center by another equivalent of Selectfluor® is also possible.
4. Facile oxidation of substrate is critical for both the iminium ion formation and hemiaminal fluorination steps.
5. In general, the Cu(I)- and previously reported [86] Ag(I)-mediated deconstructive fluorination of *N*-benzoylated cyclic amine (**LH**) by Selectfluor® proceeds through similar mechanisms. In comparison to the Ag(I)-mediated reaction, for the Cu(I)-mediated process, (a) iminium ion formation and hemiaminal fluorination have smaller energy barriers, and (b) product release and catalyst re-generation are the most energy demanding steps.

ASSOCIATED CONTENT

Supporting Information. Cartesian coordinates of all reported structures, and Figures S1–S7.

AUTHOR INFORMATION

Corresponding Author

dmusaev@emory.edu

NOTES

The authors declare no competing financial interests.

Ethical statement.

ACKNOWLEDGMENT

This work was supported by the National Science Foundation under the CCI Center for Selective C–H Functionalization (CHE-1700982). R.S. is grateful to the NIGMS (R35 GM130345A) for support of the experimental work that was the basis for this computational study. The authors gratefully acknowledge the use of the resources of the Cherry Emerson Center for Scientific Computation at Emory University. J.B.R. thanks Bristol-Myers Squibb for a graduate fellowship.

REFERENCES

1. Musaev DG, Figg TM, Kaledin AL (2014) Versatile reactivity of Pd-catalysts: mechanistic features of the mono-N-protected amino acid ligand and cesium-halide base in Pd-catalyzed C–H bond functionalization. Chem. Soc. Rev. 43: 5009-5031
2. Sperger T, Sanhueza IA, Kalvet I. Schoenebeck F (2015) Computational Studies of Synthetically Relevant Homogeneous Organometallic Catalysis Involving Ni, Pd, Ir, and Rh: An Overview of Commonly Employed DFT Methods and Mechanistic Insights. Chem. Rev. 115: 9532-9586.
3. Yang YF, Hong X, Yu JQ, Houk KN (2017) Experimental-Computational Synergy for Selective Pd(II)-Catalyzed C-H Activation of Aryl and Alkyl Groups. Acc. Chem. Res., 50: 2853-2860.
4. Chen G, Gong W, Zhuang Z, Andra MS, Chen YQ, Hong X, Yang YF, Liu T, Houk KN, Yu JQ (2016) Ligand-Accelerated Enantioselective Methylene C(sp3)-H Bond Activation, Science, 353: 1023-1027.
5. Yang YF, Chen G, Hong X, Yu JQ, Houk KN (2017) The Origins of Dramatic Differences in Five-Membered vs Six-Membered Chelation of Pd(II) on Efficiency of C(sp3)-H Bond Activation. J. Am. Chem. Soc. 139: 8514-8521.
6. Besora M, Olmos A, Gava R, Noverges B. Asensio G, Caballero A, Maseras F, Pérez PJ (2020) A quantitative model for alkane nucleophilicity based on C−H bond structural/topological descriptors. Angew. Chem. Int. Ed. 59: 3112-3116.
7. Funes-Ardoiz I, Maseras F (2018) Oxidative Coupling Mechanisms: Current State of Understanding. ACS Catalysis. 8: 1161-1172.
8. Qi X, Wang J, Dong Z, Dong G, Liu P (2020) Compatibility Score for Rational Electrophile Selection in Pd/NBE Cooperative Catalysis. Chem. 6: 2810–2825.
9. Jiang HJ, Zhong XM, Yu, J.; Zhang Y, Zhang X, Wu YD, Gong LZ (2019) Assembling a Hybrid Pd Catalyst from a Chiral Anionic CoIII Complex and Ligand for Asymmetric C(sp^3)−H Functionalization. Angew. Chem., Int. Ed. 58: 1803−1807.

10. Cheng GJ, Yang YF, Liu P, Chen P, Sun TY, Li G, Zhang X, Houk KN, Yu JQ, Wu YD (2014) Role of *N*-Acyl Amino Acid Ligands in Pd(II)-Catalyzed Remote C–H Activation of Tethered Arenes. J. Am. Chem. Soc. 136: 894–897.

11. Davies DL, Macgregor SA, McMullin CL (2017) Computational Studies of Carboxylate-Assisted C–H Activation and Functionalization at Group 8–10 Transition Metal Centers. Chem. Rev. 117: 8649–8709

12. Gorelsky SI (2013) Origins of regioselectivity of the palladium-catalyzed (aromatic) CH bond metalation-deprotonation. Coord. Chem. Rev., 257: 153-164.

13. McLarney BD, Hanna S, Musaev DG, France S (2019) Predictive model for the [$Rh_2(esp)_2$]-catalyzed intermolecular C(sp^3)–H bond insertion of β-carbonyl ester carbenes: interplay between theory and experiment. ACS Catalysis. 9: 4526-4538.

14. Kaledin A, Shi BF, Yu JQ, Key Mechanistic Features of Enantioselective C-H Bond Activation Reactions Catalyzed by [(Chiral Mono-N-Protected Amino Acid)-Pd(II)] Complexes. J. Am. Chem. Soc. 134: 1690–1698.

15. Haines BE, Musaev DG (2015) Factors Impacting the Mechanism of the Mono-N-Protected Amino Acid Ligand-Assisted and Directing-Group-Mediated C–H Activation Catalyzed by Pd (II) Complex. ACS Catalysis. 5: 830–840.

16. Haines BE, Xu HY, Verma P, Wang X, Yu JQ, Musaev DG (2015) Mechanistic Details of Pd(II)-Catalyzed C–H Iodination with Molecular I2: Oxidative Addition vs Electrophilic Cleavage. J. Am. Chem. Soc. 137: 9022–9031.

17. Haines BE, Berry JF, Yu JQ, Musaev DG (2016) Factors Controlling Stability and Reactivity of Dimeric Pd (II)-Complexes in C–H Functionalization Catalysis. ACS Catalysis 6: 829–839.

18. Haines BE, Yu JQ, Musaev DG (2017) Enantioselectivity Model for Pd-Catalyzed C–H Functionalization Mediated by the Mono-N-Protected Amino Acid (MPAA) Family of Ligands. ACS Catalysis 7: 4344–4354.

19. Cheng GJ, Chen P, Sun TY, Zhang XH, Yu JQ, Wu YD (2015) A Combined IM-MS/DFT Study on [Pd(MPAA)]-Catalyzed Enantioselective C-H Activation: Relay of Chirality Through a Rigid Framework. Chem. Eur. J. 21: 11180–11188.

20. Zhang X, Chung LW, Wu YD (2016) New Mechanistic Insights on the Selectivity of Transition-Metal-Catalyzed Organic Reactions: the Role of Computational Chemistry. Acc. Chem. Res. 49: 1302–1310.

21. Kim HT, Ha H, Kang G, Kim OS, Ryu H, Biswas AK, Lim SM, Baik MH, Joo JM (2017) Ligand-Controlled Regiodivergent C−H Alkenylation of Pyrazoles and Its Application to the Synthesis of Indazoles. Angew. Chem. Int. Ed. 56: 16262–16266.

22. Heo J, Ahn H, Won J, Son JG, Shon HK, Lee TG, Han SW, Baik MH (2020) Electro-inductive effect: Electrodes as functional groups with tunable Electronic properties", Science, 370: 214-219.

23. Liao K, Negretti S, Musaev DG, Bacsa J, Davies HML (2016) Site-Selective and Stereoselective Functionalization of Unactivated C-H Bonds. Nature, 533: 230–234.

24. Qin CM, Boyarskikh V, Hansen JH, Hardcastle KI, Musaev DG, Davies HML (2011) D_2-Symmetric Dirhodium Catalyst Derived from a 1,2,2-Triarylcyclopropanecarboxylate Ligand: Design, Synthesis and Application. J. Am. Chem. Soc. 133: 19198-19204.

25. Liao KB, Yang YF, Lie YZ, Sanders JN, Houk KN, Musaev DG, Davies HML (2018) Design of Catalysts for Site-Selective and Enantioselective Functionalization of Non-Activated Primary C-H Bonds. Nature Chem. 10: 1048-1055.

26. Liao K, Pickel TC, Boyarskikh V, Bacsa J, Musaev DG, Davies HML (2017) Site-Selective and Stereoselective Functionalization of Non-activated Tertiary C-H Bonds. Nature 551: 609-613.

27. Kisan HK, Sunoj RB (2015) Axial Coordination Dichotomy in Dirhodium Carbenoid Catalysis: A Curious Case of Cooperative Asymmetric Dual-Catalytic Approach Toward Amino Esters. J. Org. Chem. 80: 2192-2197.

28. Liu H, Duan JX, Qu DY, Guo LP, Xie ZZ (2016) Mechanistic Insights into Asymmetric C-H Insertion Cooperatively Catalyzed by a Dirhodium(II) Complex and Chiral Phosphoric Acid. Organometallics 35: 2003-2009.

29. Fu JT, Ren Z, Bacsa J, Musaev DG, Davies HML (2018) Desymmetrization of Cyclohexanes by Site- and Stereoselective C-H Functionalization. Nature, 564: 395-397

30. Gair JJ, Haines BE, Filatov AS, Musaev DG, Lewis JC (2017) Mono- N -Protected Amino Acid Ligands Stabilize Dimeric Palladium(II) Complexes of Importance to C–H Functionalization. Chem. Sci. 8: 5746–5756.

31. Xu LP, Rogue JB, Sarpong R, Musaev DG (2020) Reactivity and Selectivity Controlling factors in the Pd/diakylbiarylphosphine-catalyzed C–C cleavage/cross-coupling of an *N*-fused bicyclo α-hydroxy-β-lactam", J. Am. Chem. Soc., 142: 21140-21152

32. Salazar CA, Flesch, KN, Haines, BE, Zhou, PS, Musaev, DG, Stahl, SS (2020) Palladium-catalyzed C–H oxidative arylation accessing high turnover with O2. Science, 370: 1454-1460.

33. Xu LP, Haines BE, Ajitha, MJ, Murakami K, Itami K, Musaev DG (2020) Roles of Base in the Pd-Catalyzed Annulative Chlorophenylene Dimerization. ACS Catalysis, 10: 3059-3073.

34. Haines BE, Sarpong R, Musaev DG (2018) On the Generality and Strength of Transition Metal β–effects", J. Am. Chem. Soc. 140: 10612-10618.

35. Usui K, Haines BE, Musaev DG, Sarpong R (2018) Understanding C–H functionalization site-selectivity in a directed alkynylation, ACS Catalysis 8: 4516-4527.

36. Haines BE, Yu JQ, Musaev DG (2018) The Mechanism of Directed Ni(II)-Catalyzed C–H Iodination with Molecular Iodine. Chem. Sci. 9: 1144-1154

37. Haines BE, Yu JQ, Musaev DG (2017) An enantioselectivity model for Pd-catalyzed C-H Functionalization Mediated by the Mono-*N*-Protected Amino Acid (MPAA) Family of Ligands. ACS Catalysis 7: 4344-4354

38. Gair JJ, Haines BE, Filatov AS, Musaev DG, Lewis JC (2017) Remarkable dimeric structural motif of Palladium (II) mono-N-protected amino acid complexes and its importance in C-H Functionalization. Chem. Sci. 8: 5746-5756.

39. Plata RE, Hill DE, Haines BE, Musaev DG, Chu L, Hickey DP, Sigman MS, Yu JQ, Blackmond DG (2017) A Role for Pd(IV) in Catalytic Enantioselective C-H Functionalization With Monoprotected Amino Acid Ligands Under Mild Conditions. J. Am. Chem. Soc. 139: 9238-9245

40. Varela-Álvarez A, Yang T, Jennings H, Kornecki KP, MacMillan SN, Lancaster KM, Mack JBC, Du Bois J, Berry JF, Musaev DG (2016) Rh_2(II,III) Catalysts with Chelating Carboxylate and Carboxamidate Supports: Electronic Structure and Nitrene Transfer Reactivity. J. Am. Chem. Soc. 138: 2327-2341.

41. HainesBE, Saito Y, Segawa Y, Itami K, Musaev DG (2016) Flexible Reaction Pocket on Bulky Diphosphine-Ir Complex Controls Regioselectivity in *para*-selective C-H Borylation of Arenes. ACS Catalysis 6: 7536-7546.

42. Reyes RL, Sato M, Iwai T, Suzuki K, Maeda S, Sawamura M (2020 Asymmetric remote C–H borylation of aliphatic amides and esters with a modular iridium catalyst. Science 369: 970-974.

43. Muto K, Yamaguchi J, Musaev DG, Itami K (2015) Decarbonylative organoboron cross-coupling by nickel catalysis. The ester Suzuki–Miyaura coupling. Nature Communication 6: 1-8

44. Figg TM, Park S, Park J, Chang S, Musaev DG (2014) Comparative Mechanistic Investigations of Direct C–H Amination of Benzamides Catalyzed by Cp*-Based Group 9 Metal Complexes. Organometallics 33: 4076–4085.

45. Xu H, Muto K, Yamaguchi J, Zhao C, Itami K, Musaev DG (2014) Key Mechanistic Features of Ni-catalyzed C–H/C–O Biaryl Coupling of Azoles and Naphthalen-2-yl Pivalates. J. Am. Chem. Soc. 136: 14834-14844.

46. Figg TM, Wasa M, Yu JQ, Musaev DG (2013) Understanding the reactivity of Pd(0)/PR_3 catalyzed intermolecular C(sp^3)-H bond arylation. J. Am. Chem. Soc. 135: 14206–14214.

47. Varela-Álvarez A, Musaev DG (2013) Can the bis(imino)pyridine Iron, (PDI)FeL^1L^2, Complex Catalyze C-H Bond Functionalization ? Chem Sci. 4: 3758-3764

48. Davies HML, Beckwith REJ (2003) Catalytic Enantioselective C-H Activation by Means of Metal-Carbenoid-Induced C-H Insertion. Chem. Rev. 103: 2861-2904.

49. Giri R, Shi BF, Engle KM, Maugel N, Yu JQ (2009) Transition metal-catalyzed C–H activation reactions: diastereoselectivity and enantioselectivity. Chem. Soc. Rev. 38: 3242-3272.

50. Doyle MP, Duffy R, Ratnikov M, Zhou L (2010) Catalytic Carbene Insertion into C–H Bonds. Chem. Rev. 110: 704-724.

51. Lyons TW, Sanford MS (2010) Palladium-catalyzed ligand-directed C−H functionalization reactions. Chem. Rev. 110: 1147-1169;

52. Davies HML, Morton D (2011) Guiding Principles for Site Selective and Stereoselective Intermolecular C-H Functionalization by Donor/acceptor Rhodium Carbenes. Chem. Soc. Rev. 40: 1857-1869.

53. Wencel-Delord J, Dröge T, Liu F, Glorius F (2011) Towards mild metal-catalyzed C–H bond activation. Chem. Soc. Rev. 40: 4740-4761.

54. Gutekunst WR, Baran PS (2011) C–H functionalization logic in total synthesis. Chem. Soc. Rev. 40: 1976-1991

55. Ackermann L (2011) Carboxylate-assissted transition-metal-catalyzed C–H functionalization: mechanism and scope. Chem. Rev. 111: 1315-1345.

56. Bruckl T, Baxter RD, Ishihara Y, Baran PS (2012) Innate and Guided C—H Functionalization Logic. Acc. Chem. Res. 45: 826-839.

57. Hartwig JF, Larsen MA (2016) Undirected, Homogeneous C—H Bond Functionalization: Challenges and Opportunities. ACS Cent. Sci. 2: 281-292.

58. Cernak T, Dykstra KD, Tyagarajan S, Vachal P, Krska SW (2016) The Medicinal Chemist's Toolbox for Late-Stage Functionalization of Drug-Like Molecules. Chem. Soc. Rev. 45: 546–576.

59. Engle KM (2016) The Mechanism of Palladium (II)-Mediated C–H Cleavage with Mono-N-Protected Amino Acid (MPAA) Ligands: Origins of Rate Acceleration. Pure and Applied Chemistry 88: 119-138.

60. Hartwig JF (2017) Catalyst-Controlled Site-Selective Bond Activation. Acc. Chem. Res. 50: 549-555.

61. Gandeepan P, Muller T, Zell D, Cera G, Warratz S, Ackermann L (2019) 3d Transition metals for C-H activation. Chem. Rev. 119: 2192-2452.

62. Davies HML, Liao KB, (2019) Dirhodium Tetracarboxylates as Catalysts for Selective Intermolecular C—H Functionalization. Nat. Rev. Chem. 3: 347-360.

63. Morton CM, Zhu QL, Ripberger H, Troian-Gautier L, Toa ZSD, Knowles RR, Alexanian EJ (2019) C–H Alkylation via Multisite-Proton-Coupled Electron Transfer of an Aliphatic C-H Bond. J. Am. Chem. Soc. 141: 13253-13260.

64. Yamaguchi J, Yamaguchi AD, Itami K (2012) C–H bond functionalization: Emerging Synthetic tools for natural products and pharmaceuticals. Angew. Chem. Int. Ed. 51: 8960-9009.

65. Wang B, Perea MA, Sarpong R. (2020) Transition Metal-Mediated C−C Single Bond Cleavage: Making the Cut in Total Synthesis. Angew. Chem. Int. Ed. 59: 18898−18919.

66. Murakami M, Ishida N (2016) Potential of Metal-Catalyzed C−C Single Bond Cleavage for Organic Synthesis. J. Am. Chem. Soc. 138: 13759−13769.

67. Tsui E, Wang H, Knowles RR (2020) Catalytic Generation of Alkoxy Radicals from Unfunctionalized Alcohols. Chem. Sci. 11: 11124−11141.

68. Guo JJ, Hu A, Zuo Z (2018) Photocatalytic alkoxy radical- mediated transformations. Tetrahedron Lett. 59: 2103−2111.

69. Xia Y, Dong G (2020) Temporary or removable directing groups enable activation of unstrained C–C bonds. Nature Reviews Chem. 4: 600-614.

70. Chen F, Wang T, Jiao N (2014) Recent Advances in Transition-Metal-Catalyzed Functionalization of Unstrained Carbon–Carbon Bonds. Chem. Rev. 114: 8613–8661.

71. Differding E, Lang RW (1988) New fluorination reagents-I. The first enantioselective fluorination reaction. Tetrahedron Lett. 29: 6087−6090.

72. Umemoto T, Kawada K, Tomita K (1986) N-fluoropyridinium triflate and its derivatives: Useful fluorinating agents. Tetrahedron Lett. 27: 4465−4468.

73. Davis FA, Han W (1991) N-fluoro-o-benzenedisulfonimide: a useful new fluorinating reagent. Tetrahedron Lett. 32: 1631−1634.

74. Banks RE (1998) Selectfluor™ reagent F-TEDA-BF_4 in action: tamed fluorine at your service. J. Fluorine Chem. 87: 1−17 and references cited therein.

75. Stavber S (2011) Recent Advances in the Application of Selectfluor™ F-TEDA-BF_4 as a Versatile Mediator or Catalyst in Organic Synthesis. Molecules 16: 6432−6464.

76. Vincent SP, Burkart MD, Tsai CY, Zhang Z, Wong CH (1999) Electrophilic Fluorination−Nucleophilic Addition Reaction Mediated by Selectfluor: Mechanistic Studies and New Applications. J. Org. Chem. 64: 5264−5279.

77. Oliver EW, Evans DH (1999) Electrochemical studies of six N–F electrophilic fluorinating reagents. J. Electroanal. Chem. 474: 1−8.

78. Kawakami T, Murakami K, Itami K (2015) Catalytic C–H imidation of aromatic cores of functional molecules: Ligand-accelerated Cu catalysis and application to materials- and biology-oriented aromatics. J. Am. Chem. Soc. 137: 2460-2463.

79. Haines BE, Kawakami T, Murakami K, Itami K, Musaev DG (2017) Key Mechanistic Details and predictive Models for Cu-catalyzed Aromatic C-H Imidation with *N*-Fluorobenzenesulfonimide. Chem. Sci. 8: 988-1002

80. Pitts CR, Bloom S, Woltornist R, Auvenshine DJ, Ryzhkov LR, Siegler MA, Lectka T (2014) Direct, Catalytic Monofluorination of sp^3 Bonds: A Radical-Based Mechanism with Ionic Selectivity. J. Am. Chem. Soc. 136: 9780-9791.

81. Rueda-Becerril M, Sazepin CC, Leung JCT, Okbinoglu T, Kennepohl P, Paquin JF, Sammis GM (2012) Fluorine Transfer to Alkyl Radicals. J. Am. Chem. Soc. 134: 4026−4029.

82. Michaudel Q, Thevenet D, Baran PS (2012) Intermolecular Ritter-Type C–H Amination of Unactivated sp^3-Carbons. J. Am. Chem. Soc. 134: 2547-2550.

83. Roque JB, Kuroda Y, Göttemann LT, Sarpong R. (2018) Deconstructive Diversification of Cyclic Amines. Nature 564: 244-248.

84. Roque JB, Kuroda Y, Göttemann LT, Sarpong R. (2018) Deconstructive Fluorination of Cyclic Amines by Carbon-Carbon Cleavage. Science 361: 171-174.

85. Roque JB, Kuroda Y. Jurczyk J, Xu LP, Ham JS, Göttemann LT, Roberts C, Adpressa D, Saurí J, Joyce LA, Musaev DG, Yeung CS, Sarpong R. (2020) C–C cleavage approach to C–H functionalization of saturated aza-cycles. ACS Catalysis 10: 2929–2941.

86. Roque JB, Sarpong R, Musaev DG (2021) Key Mechanistic Features of a Silver(I)-Mediated Deconstructive Fluorination of Cyclic Amines: Multi-State Reactivity versus Single Electron Transfer. J. Am. Chem. Soc., 143: https://doi.org/10.1021/jacs.0c13061

87. Murakami M, Ishida N (2016) Potential of Metal-Catalyzed C–C Single Bond Cleavage for Organic Synthesis. J. Am. Chem. Soc. 138: 13759–13769.

88. O'Reilly ME, Dutta S, Veige AS (2016) β-Alkyl Elimination: Fundamental Principles and Some Applications. Chem. Rev. 116: 8105– 8145.

89. Souillart L, Cramer N (2015) Catalytic C–C Bond Activations via Oxidative Addition to Transition Metals. Chem. Rev. 115: 9410–9464.

90. Yu C, Shoaib MA, Iqbal N, Kim JS, Ha HJ, Cho EJ (2017) Selective Ring-Opening of *N*-Alkyl Pyrrolidines with Chloroformates to 4-Chlorobutyl Carbamates. J. Org. Chem. 82: 6615–6620.

91. Feraldi-Xypolia A, Gomez Pardo D, Cossy J (2015) Ring Contraction of 3-Hydroxy-3 (trifluoromethyl)piperidines: Synthesis of 2-Substituted 2-(Trifluoromethyl)pyrrolidines. Chem. Eur. J. 21: 12876–12880.

92. Wang F, He Y, Tian M, Zhang X, Fan X (2018) Synthesis of α-Formylated *N*-Heterocycles and Their 1,1-Diacetates from Inactivated Cyclic Amines Involving an Oxidative Ring Contraction, Org. Lett. 20: 864–867.

93. Huang FQ, Xie J, Sun JG, Wang YW, Dong X, Qi LW, Zhang B (2016) Regioselective Synthesis of Carbonyl-Containing Alkyl Chlorides via Silver-Catalyzed Ring-Opening Chlorination of Cycloalkanols. Org. Lett. 18: 684–6877.

94. Zhao H, Fan X, Zhu C (2015) Silver-Catalyzed Ring-Opening Strategy for the Synthesis of β- and γ-Florinated Ketons. J. Am. Chem. Soc. 137: 3490-3493.

95. Patel NR, Flowers III R A (2015) Mechanistic Study of Silver-Catalyzed Decarboxylative Fluorination. J. Org. Chem. 80: 5834-5841.

96. Yayla HG, Wang H, Tarantino KT, Orbe HS, Knowles RR (2016) Catalytic Ring-Opening of Cyclic Alcohols Enabled by PCET Activation of Strong O–H Bonds. J. Am. Chem. Soc. 138: 10794-10797.

97. Yin F, Wang Z, Li Z, Li C (2012) Silver-Catalyzed Decarboxylative Fluorination of Aliphatic Carboxylic Acids in Aqueous Solution. J. Am. Chem. Soc. 134: 10401-10404.

98. Huang X, Hooker JM, Groves JT (2015) Targeted Fluorination with the Fluoride Ion by Manganese-Catalyzed Decarboxylation. Angew. Chem. Int. Ed. 54: 5241-5245.

99. Brandt JR, Lee E, Boursalian GB, Ritter T (2014) Mechanism of Electrophilic Fluorination with Pd(IV): Fluoride Capture and Subsequent Oxidative Fluoride Transfer. Chem Sci. 5: 169-179.

100. Hua A M, Mai DN, Martinez R, Baxter RD (2017) Radical C–H fluorination using unprotected amino acids as radical precursors. Org. Lett. 19: 2949-2952.

101. Schroder D, Shaik S, Schwarz H (2000) Two-state reactivity as a new concept in organometallic chemistry. Acc. Chem. Res. 33: 139-145.

102. de Visser SP, Ogliaro F, Harris N, Shaik S (2001) Epoxidation of Ethene by Cytochrome P450: A Quantum Chemical Study. J. Am. Chem. Soc. 123: 3037-3047.

103. Klinker E J, Shaik S, Hirao H, Que Jr. L (2009) Two-state reactivity model explains unusual kinetic isotope effect patterns in CH bond cleavage by non-heme oxoiron(IV) complexes. Angew. Chem. Int. Ed. 48: 1291-1297.

104. Musaev DG, Morokuma K. (1993) Ab Initio molecular orbital study of the electronic and geometrical structure of MCH_2^+ and the reaction mechanism: $MCH_2^+ + H_2 \rightarrow M^+ + CH_4$, (M = Co, Rh and Ir). Isr. J. Chem. 33: 307-316.

105. Musaev DG, Morokuma K (1996) Molecular orbital study of the mechanism of Sc^+ with methane. Comparison of the reactivity of early and late first-row transition metal cations and their carbene complexes. J. Phys. Chem. 100: 11600-11609.

106. Musaev DG, Morokuma K. (1996) Potential energy surface of transition metal catalyzed chemical reactions. Adv. Chem. Phys. 61-128.

107. Musaev DG, Morokuma K, Koga N, Nguyen KA, Gordon MS, Cundari TR (1993) An Ab Initio study of the molecular and electronic structure of $CoCH_2^+$ and the reaction mechanism: $CoCH_2^+ + H_2$. J. Phys. Chem. 97: 11435-11444.

108. Musaev DG, Koga N, Morokuma K. (1993) Ab Initio molecular orbital study of the electronic and geometrical structure of $RhCH_2^+$ and the reaction mechanism: $RhCH_2^+ + H_2 \rightarrow Rh^+ + CH_4$. J. Phys. Chem. 97: 4064-4075.

109. Yarkony D. (1996) Diabolical Conical Intersections. Rev. Modern Physics 68: 985–1013

110. Based on the DFT calculations alone we cannot confidently eliminate a fluoro-cation coupled electron transfer (FCCET) character of this step.

111. Frisch MJ, et. al. (2019) *Gaussian 16, Revision C.01*, Gaussian, Inc., Wallingford CT USA.

112. Hay PJ, Wadt WR (1985) Ab Initio Effective Core Potentials for Molecular Calculations. Potentials for the Transition Metal Atoms Sc to Hg. J. Chem. Phys. 82: 270-283.

113. Hay PJ, Wadt WR (1985) Ab Initio Effective Core Potentials for Molecular Calculations. Potentials for K to Au Including the Outermost Core Orbitals. J. Chem. Phys. 82: 299-310.

114. Hay PJ, Wadt WR (1985) Ab Initio Effective Core Potentials for Molecular Calculations. Potentials for Main Group Elements Na to Bi. J. Chem. Phys. 82: 284-298.

115. Becke AD (1988) Density-Functional Exchange-Energy Approximation with Correct Asymptotic Behavior. Phys. Rev. A 38: 3098-3100.

116. Lee C, Yang W, Parr RG (1988) Development of The Colle-Salvetti Correlation-Energy Formula into a Functional of the Electron Density. Phys. Rev. B 37: 785-789.

117. Becke AD (1993) A New Mixing of Hartree–Fock and Local Density-Functional Theories. J. Chem. Phys. 98: 1372-1377.

118. Grimme S, Antony J, Ehrlich S, Krieg, HA (2010) Consistent and Accurate Ab Initio Parametrization of Density Functional Dispersion Correction (DFT-D) for the 94 Elements H-Pu. *J. Chem. Phys. 132*: 154104-154122.

119. Becke AD, Johnson ER (2005) A Density-Functional Model of the Dispersion Interaction. J. Chem. Phys. 123: 154101-154106.

120. Becke AD, Johnson ER (2005) Exchange-Hole Dipole Moment and the Dispersion Interaction. J. Chem. Phys. 122: 154104-154109.

121. Johnson ER, Becke AD (2006) A Post-Hartree-Fock Model of Intermolecular Interactions: Inclusion of Higher-Order Corrections. J. Chem. Phys. 124: 174104-174112.

122. Hamill LA, Snyder JD, Ess DH (2016) MECPro Version 1.0.3: Minimum Energy Crossing Program.

123. Barone V, Cossi M (1998) Quantum Calculation of Molecular Energies and Energy Gradients in Solution by a Conductor Solvent Model. J. Phys. Chem. A 102: 1995-2001.

124. Cossi M, Rega N, Scalmani G, Barone V (2003) Energies, Structures, and Electronic Properties of Molecules in Solution with the C-PCM Solvation Model. J. Comput. Chem. 24: 669-681.

125. Pritchard BP, Altarawy D, Didier B, Gibson TD, Windus TL (2019) A New Basis Set Exchange: An Open, Up-to-date Resource for the Molecular Sciences Community. J. Chem. Inf. Model. 59: 4814-4820

126. Chai JD, Head-Gordon M (2008) Long-range Corrected Hybrid Density Functionals with Damped Atom-Atom Dispersion Corrections. Phys. Chem. Chem. Phys. 10: 6615-6620;

127. Previously, [86] we have validated the use of dication $(F\text{-}TEDA)^{2+}$, without the two corresponding BF_4-counter anions, as a model for Selectfluor®.

128. At the [B3LYP-D3(BJ)+PCM]/[cc-pVTZ + Lanl2dz(f) (Cu)] and [wB97XD+PCM]/[cc-pVTZ + Lanl2dz(f) (Cu)] levels of theory the calculated: (a) exothermicity of the reaction (1) is 9.8/11.0 and 5.0/6.3 kcal/mol, (b) complexation energy of intermediate $Cu(I)[F\text{-}TEDA]^{2+}$ is -6.8/3.4 and -6.5/3.3 kcal/mol, and (c) Cu(II)F dimerization energy is 43.0/29.7 and 41.0/27.7 kcal/mol, respectively.

129. At the [B3LYP-D3(BJ)+PCM]/[cc-pVTZ + Lanl2dz(f)(Cu)] and [wB97XD+PCM]/[cc-pVTZ + Lanl2dz(f)(Cu)] levels of theory the calculated: (a) energy of the reaction **LH** + Cu(I) → [(**LH**)–Cu(I)] is 35.9/26.1 and 33.3/22.7 kcal/mol, (b) exothermicity of the reaction (2) is 10.6/10.3 and 5.6/6.2 kcal/mol, and (c) complexation energy of intermediate $[(\mathbf{LH})\text{–}Cu(I)][F\text{-}TEDA]^{2+}$ is -9.8/+4.2 and -9.3/+3.1 kcal/mol, respectively.

130. See, NIST: Atomic Spectra Database – Ionization Energies Form https://physics.nist.gov/PhysRefData/ASD/ionEnergy.html